

Subglacial channels, climate warming, and increasing frequency of Alpine glacier snout collapse

Pascal Emanuel Egli¹, Bruno Belotti², Boris Ouvry³, James Iving¹, and Stuart N Lane⁴

¹University of Lausanne

²Department of Geological Sciences, University of Idaho

³Institute of Geography, University of Zurich

⁴Université de Lausanne

November 22, 2022

Abstract

Alpine glacier retreat has increased markedly since the late 1980s, and is commonly linked to the effects of rising temperature on surface melt. Less considered are processes associated with glacier surface collapse. A survey of 22 retreating Swiss glaciers suggests that snout marginal collapse events have increased in frequency since the late 1980s, driven by ice thinning and reductions in glacier-longitudinal ice flux. Detailed measurement of a collapse event at one glacier showed vertical deformation of the surface above the main subglacial channel. But with low rates of longitudinal flux and vertical creep closure, this was insufficient to close the channel in the snout marginal zone. We hypothesise that this maintains contact between subglacial ice and the atmosphere, allowing greater incursion of warm air up-glacier, thus enhancing melt from below. The associated enlargening of subglacial channels at glacier snouts leads to surface collapse and removal of ice via fluvial processes.

Hosted file

supporting_information_egli_etal.docx available at <https://authorea.com/users/536735/articles/599179-subglacial-channels-climate-warming-and-increasing-frequency-of-alpine-glacier-snout-collapse>

1
2
3
4 **Subglacial channels, climate warming, and**
5 **increasing frequency of Alpine glacier snout collapse**

6 **Pascal E. Egli^{1*}, Bruno Belotti², Boris Ouvry³, James Irving⁴, Stuart N. Lane¹**

7 ¹ Institute of Earth Surface Dynamics, University of Lausanne, Switzerland

8 ² Department of Geological Sciences, University of Idaho, Idaho, USA

9 ³ Institute of Geography, University of Zurich, Switzerland

10 ⁴ Institute of Earth Sciences, University of Lausanne, Switzerland

11 Corresponding author: Pascal Egli (eglipascal@gmx.net)

12 **Key Points:**

- 13 • A survey of 22 Alpine glaciers shows increased margin collapse frequency linked to
14 rapid climate warming since the 1980s
 - 15 • Collapse appears to be associated with glacier thinning, stagnation of snout
16 margins and reduced rates of subglacial channel closure
 - 17 • Glaciers with collapse features have retreat rates that are more sensitive to inter-
18 annual temperature fluctuations
 - 19 • Intensive study of a collapse event confirms that significant up-glacier extension of
20 an unpressurised subglacial channel drives the collapse process
- 21

Abstract

Alpine glacier retreat has increased markedly since the late 1980s, and is commonly linked to the effects of rising temperature on surface melt. Less considered are processes associated with glacier surface collapse. A survey of 22 retreating Swiss glaciers suggests that snout marginal collapse events have increased in frequency since the late 1980s, driven by ice thinning and reductions in glacier-longitudinal ice flux. Detailed measurement of a collapse event at one glacier showed vertical deformation of the surface above the main subglacial channel. But with low rates of longitudinal flux and vertical creep closure, this was insufficient to close the channel in the snout marginal zone. We hypothesise that this maintains contact between subglacial ice and the atmosphere, allowing greater incursion of warm air up-glacier, thus enhancing melt from below. The associated enlarging of subglacial channels at glacier snouts leads to surface collapse and removal of ice via fluvial processes.

Plain language summary

Mountain glaciers have been melting and retreating more rapidly since the onset of accelerated atmospheric warming in the late 1980s. Our study examines 22 Swiss glaciers in order to understand why for some glaciers the ice surface close to the glacier margin breaks down and forms collapse features, and for others it does not. We find that the combination of thin ice having a low surface slope results in locally reduced ice flow, which causes subglacial channels to close more slowly and eventually leads to channel roof collapse. A detailed study based on ground-penetrating radar and drone surveys at one of the glaciers showed that the subglacial channel there is very wide and shallow, and that its strongly sinuous shape may have contributed to a recent ice-surface collapse. Ice blocks from the melting and collapsing channel were flushed out by the proglacial stream. We observe that such collapse features have become more frequent with a stronger increase in air temperature. Visibly, such collapse features may contribute to more rapid glacier recession.

1 Introduction

Alpine glaciers have been retreating rapidly since the 1980s because of rapid climate warming (Salzmann et al., 2012; Huss et al., 2010; Paul & Haeberli, 2008). Retreat is forecast to accelerate in the coming decades (Zekollari et al., 2019). The primary mechanism of mass loss is surface melt. However, other mechanisms may play an important role. One of these involves the collapse of subglacial channels in the snout marginal zone, driven by thinning ice combined with slow creep closure. After collapse, the ice is removed via the channel to the glacier outlet. This mechanism of glacier retreat was first described some time ago as 'subglacial stoping' or 'block caving' (Paige, 1956; Loewe, 1957).

There are few examples where such collapse behaviour has been documented and quantified (Bartholomaus et al., 2011; Dewald et al., 2021; Kellerer-Pirklbauer & Kulmer, 2018; Konrad, 1998; Lindström, 1993; Stocker-Waldhuber et al., 2017). As a result, little is known about where and when these collapse features form and whether or not their frequency of formation is changing in response to climate warming.

We hypothesise that the formation of collapse features is driven by three interconnected mechanisms: (1) high temperatures lead to high melt rates and shallow ice in the snout marginal area of glaciers; (2) shallow ice means reduced longitudinal ice flow velocities and reduced creep closure of subglacial channels; and (3) the presence of a subglacial channel underneath shallow ice can initiate a collapse feature due to upwards melting and block caving.

In this study, we perform statistical analysis on a sample of 22 Swiss glaciers based on 24 glacier properties, climate data, and historical aerial imagery in order to investigate how pervasive these collapse events are becoming and to test the abovementioned hypotheses. The results obtained are supported by the intensive study of one retreating glacier which experienced a recent (2017-2018) collapse event, the Glacier d'Otemma. For this glacier we were able to measure ablation, surface elevation change, and the position of the corresponding subglacial channel, which allowed us to document the processes leading to the channel collapse.

85

86 **2 Materials and Methods**

87

88 **2.1 Overview**

89

90 We first examine the conditions driving snout margin collapse through the analysis of
91 topography, ice thickness, historical aerial imagery, air temperature, and glacier retreat
92 data for 22 glaciers in the western and central Swiss Alps (Figure S1). We focus on
93 Swiss glaciers because of the widespread availability of measurements, notably of
94 glacier bed topography, ice thickness, and aerial imagery, that allow us to build an
95 extensive database of the conditions at glacier snout margins. Based on historical and
96 contemporary aerial imagery, 12 glaciers were selected that were found to show at least
97 one subglacial channel collapse feature near their terminus since the first date of aerial
98 imagery in 1938. In addition, 10 glaciers not exhibiting collapse features were chosen,
99 all of them located in close vicinity to the aforementioned glaciers and having
100 comparable topography and size to nearby glaciers with collapse features, in order to
101 do a balanced statistical comparison (Figure S1).

102

103 In the second part of our study, we examine in detail the ice surface lowering, subglacial
104 channel position, and ice ablation measured using uncrewed aerial vehicle (UAV)
105 imagery, ground-penetrating radar (GPR) measurements, and ablation stakes,
106 respectively, before and during a collapse event at the Glacier d'Otemma (2017-2018).
107 This is done to investigate the mechanisms leading to such events and to reveal the
108 extent to which unpressurised subglacial marginal channels can extend up-glacier.

109

110

111

112

113

114 **2.2 Frequency of collapse events**

115

116 To test whether the frequency of snout marginal channel collapse events is increasing
117 with time, we used the SwissTopo LUBIS visualization system. LUBIS contains all of the
118 digitized aerial imagery held by SwissTopo back to 1938. We inspected the imagery
119 available for the snout region of each glacier in order to determine whether or not a
120 collapse feature was present (Figure S1). Each instance where the snout of one of the
121 glaciers was shown was counted as an observation. On some aerial images several of
122 the chosen glacier snouts were visible, meaning that the same image could be counted
123 more than once. There were 179 observations in total, of which 29 showed a collapse
124 feature and 150 did not. After eliminating multiple counts of the same collapse feature,
125 27 separate collapse events remained. The cumulative number of identified collapses
126 through time is presented alongside the cumulative number of observations made in
127 order to account for a change in the number of observations after 1980.

128

129 **2.3 Characterization of collapse conditions**

130

131 For each of the 22 glaciers considered, we assembled a database consisting of (i) surface
132 elevation information from the SwissAlti3D Digital Elevation Model (SwissTopo, 2020);
133 (ii) bed topography and ice thickness measurements based on GPR data and modelling
134 (Grab et al., 2021); and (iii) retreat history information from the Swiss Glacier
135 Monitoring Network (GLAMOS, 1885-2019). Supporting Information section 3.1 explains
136 how this database was put together and Table S2 lists the 24 properties, considered in
137 our analysis, that were derived from the data either directly (e.g., ice thickness in the
138 snout marginal zone) or inferred from basic process laws (e.g., mean snout marginal
139 glacier velocity).

140

141 To investigate the extent to which glaciers showing collapse features are likely to have
142 lower longitudinal ice flux and subglacial channel closure, we determined the mean ice
143 thickness, bed slope and surface slope for the entire glacier and for the first 2 km of

144 each glacier tongue. These parameters were also determined for a 100 m radius around
145 each of the most recent collapse zone locations. The mean distance between the center
146 of the most recent collapse feature and the glacier terminus for the 12 glaciers showing
147 collapse features was found to be ~ 250 m. Thus, for glaciers not showing collapse
148 features, a hypothetical collapse zone of 100 m radius, positioned at the centerline at a
149 horizontal distance of 250 m from the terminus, was used. Supporting Information
150 section 3.1 explains how the latter information was used to estimate the mean
151 longitudinal velocity and vertical closure rate.

152
153 We also characterized glacier retreat using GLAMOS (GLAMOS, 1881-2019) data to
154 determine length change and variability in length change since 1987, which is the date
155 considered for the onset of rapid recession related to climate warming in the study
156 region (Costa et al., 2018).

157
158 Finally, Jarque and Bera (1980) tests of the 22 samples of each property in Table S2
159 suggested that 13 out of 24 properties were non-Gaussian distributed at the 5%
160 significance level. Consequently, we used Mann and Whitney (1947) U tests to assess
161 the extent to which these properties differed between those glaciers showing channel
162 collapse and those not showing collapse.

163 164 **2.4 Relationship between summer air temperatures and retreat**

165
166 If collapse formation is driven by the incursion of warm air underneath snout margins
167 via unpressurised subglacial channels, then we might expect variation in the annual
168 snout recession to be more sensitive to mean annual summer air temperature variations
169 than for those glaciers where snout recession is driven by temperature effects on surface
170 melt alone. To investigate this hypothesis, we identified for each glacier the year of
171 onset of continuous retreat according to the GLAMOS (1881-2019) database
172 (Supporting Information section 3.7). We then calculated a time-series of annual retreat
173 rate (R_A) and its mean (R_M) for each glacier for the period during which each glacier was
174 retreating. For the same period, we determined the annual mean summer air
175 temperature in the snout region (T_{SA}) and its mean (T_{SM}). This was done using spatially

176 interpolated and gridded MeteoSwiss data (temperature 2 m above the ground between
177 June 1 and August 31) from the center of the 1x1 km grid cell located closest to the
178 glacier terminus. We determined the coefficient of variation of retreat (R_{CV}) by dividing
179 the standard deviation of retreat by the mean annual retreat rate. We computed the
180 Pearson's correlation coefficient (P_{RT}) between T_{SA} and R_A and we calculated the
181 sensitivity of R_A to T_{SA} (S_{RT}) using simple linear regression. For each of these parameters
182 a Jarque and Bera (1980) test was used to check for normality (H_0 , normal distribution,
183 could not be rejected at $p=0.05$). This allowed us to compare glaciers with and without
184 collapse features using Student's t, for all parameters except S_{RT} . The latter was not
185 normally distributed ($p<0.05$) and so we used the Mann and Whitney (1947) U test.

187 **2.5 Surface dynamics and subglacial channel collapse at the Glacier** 188 **d'Otemma**

189
190 To establish in more detail the physical processes that explain these extensive
191 inferences, we studied the process of snout marginal collapse for one of the glaciers in
192 the database, the Glacier d'Otemma (Figure S1). In 2018, this glacier had a snout
193 elevation of 2490 m and a maximum elevation of 3600 m. A collapse feature was
194 observed to be forming 210 m upstream of the glacier snout in 2017, where the glacier
195 surface slope was 10°, the glacier bed slope was 12°, and the mean ice thickness was
196 22 m. The collapse feature coincided with a major subglacial channel that became visible
197 after the collapse event in 2018. We aimed to determine the planform geometry of the
198 subglacial channel and vertical ice deformation of the snout zone.

199
200 To determine the planform geometry of the subglacial channel, during the summer of
201 2017, we acquired a series of densely spaced GPR lines over the snout zone of the
202 Glacier d'Otemma that provided us with high-resolution images of the main subglacial
203 channel location (Egli et al., 2021). The channel outline in the northeast is based on an
204 additional GPR dataset, processed in the exact same way as in Egli et al. (2021). We
205 also calculated the Shreve hydraulic potential (Shreve, 1972;; Figure S14; section 3.2
206 in Supporting Information).

208 We hypothesize that if the subglacial channel close to the glacier snout was
 209 unpressurised and large enough, then we might see greater rates of vertical deformation
 210 on the ice surface in this location due to creep, albeit insufficient to close the channel,
 211 thereby setting the preconditions for a subglacial channel collapse feature and at the
 212 same time providing a diagnostic tool of the spatial extent of unpressurised channels.
 213 Thus, to calculate vertical ice deformation, UAV surveys were undertaken for the
 214 purpose of structure from motion multi-view stereo (SfM-MVS) photogrammetry
 215 (Supporting Information section 3.2, Figures S3, S4, S5). These also allowed us to
 216 visualise the development of a collapse feature (Figure S15). We used two surveys to
 217 determine vertical deformation on the 7th of August 2018 and on the 23rd of August
 218 2018 whilst the collapse was happening. Each involved ~ 1000 images and was
 219 supported by 54 ground control points (GCPs) that were surveyed using a differential
 220 global positioning system (dGPS). Digital elevation models (DEMs) were produced
 221 applying a standard processing workflow (James et al., 2020; Rossini et al., 2018,
 222 Gindraux et al., 2017; Westoby et al., 2012; Supporting Information section 2.2; Figure
 223 S3) using the Agisoft Metashape[©] software. A DEM of difference (DoD; dz_{net}) showing
 224 the difference in surface elevation between the two surveys (16 days apart) was then
 225 computed. We did not correct the surface elevation change for lateral ice flux as the
 226 lateral velocity in the snout margin was measured by dGPS at the ablation stakes as
 227 only a few centimeters per month.

228
 229 In order to distinguish between ablation and ice dynamics, we defined the net surface
 230 height change (dz_{net}), as the sum of a component due to vertical deformation ($dz_{dynamics}$)
 231 and a component due to ablation ($dz_{ablation}$):

$$dz_{net} = dz_{dynamics} + dz_{ablation} \quad 233 \quad [1]$$

234

235 The ablation component ($dz_{ablation}$) was estimated from manual measurement of melt
 236 for 49 stakes distributed across the area. These measurements were interpolated
 237 spatially using kriging to yield $dz_{ablation}$. The latter was subtracted from dz_{net} to derive
 238 the surface change due to ice dynamics, $dz_{dynamics}$ (Supporting Information section 3.3).

239 To test for the influence of variables such as aspect, reflectance, slope or debris cover
240 on ice surface elevation change and melt we computed their correlations with dz_{net} and
241 $dz_{ablation}$ (Figure S7, S8, Table S4). As a proxy for the albedo we looked at surface
242 reflectance as a measure for the fraction of short wave radiation reflected (Rippin et al.,
243 2015).

244
245 Finally, we tested for a relationship between the presence of a subglacial channel and
246 patterns of increased ice surface elevation change. Based on the GPR-derived channel
247 outlines and on the Shreve hydraulic potential (Figure S14), the ablation stakes were
248 classified according to the likelihood that they were located on top of a subglacial
249 channel in order to assess the importance of the presence of a subglacial channel for
250 ice surface lowering (Supporting Information section 3.8; Figure 3a-d).

251 252 **3 Results**

253 254 **3.1 Collapse events and their changing frequency**

255
256 Figure 1 shows the most recent channel collapse features identified in aerial imagery
257 for the different glaciers considered. They differ in the detail of their form, but most
258 have concentric crevasse-like features present in both the early stages of development
259 (e.g. Figure 1c, 1i), during collapse (e.g. Figure 1a) and afterwards (e.g. Figure 1e, 1j).
260 The images confirm that these features can develop in both debris-free and debris-
261 covered snout marginal zones.

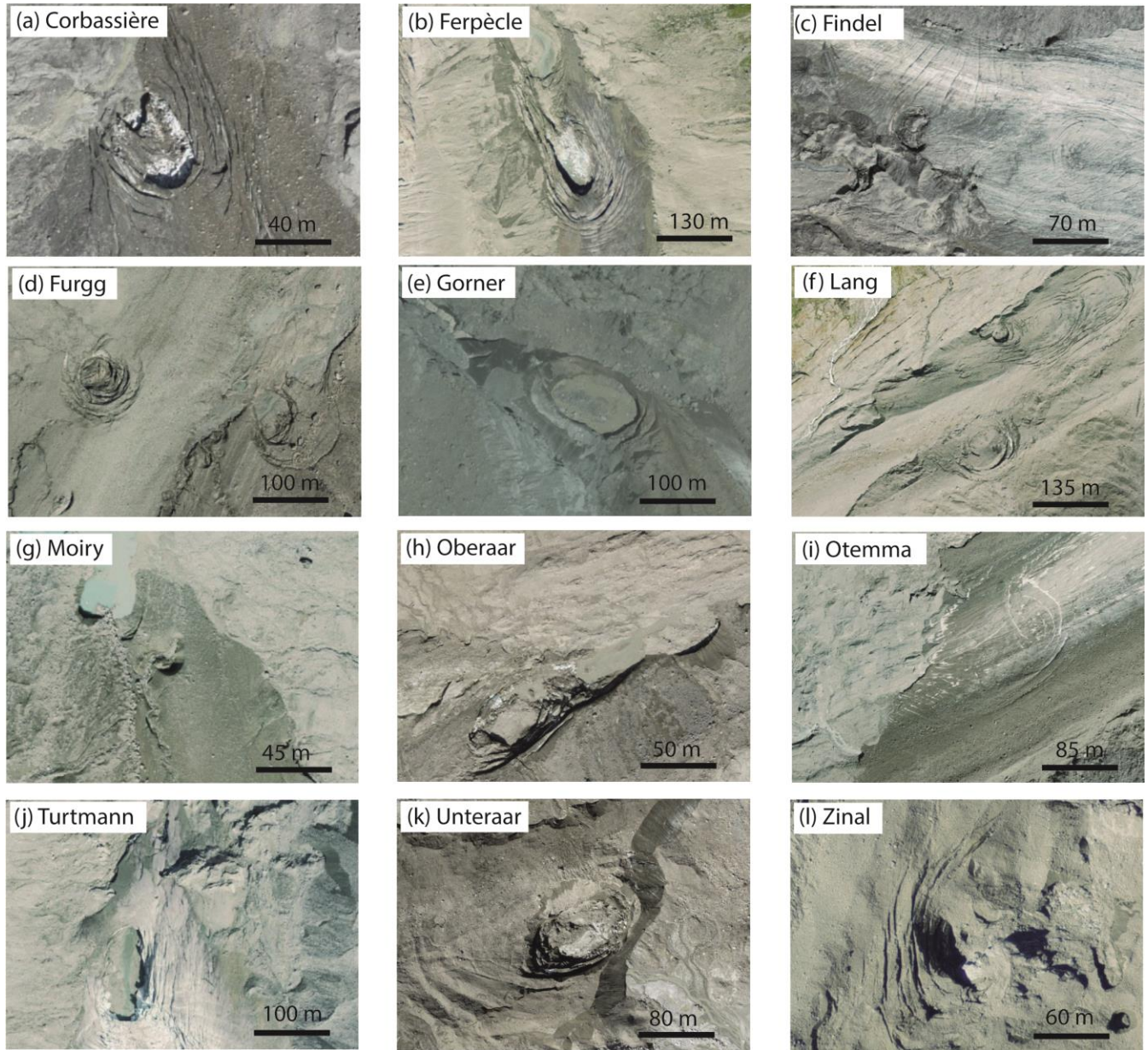
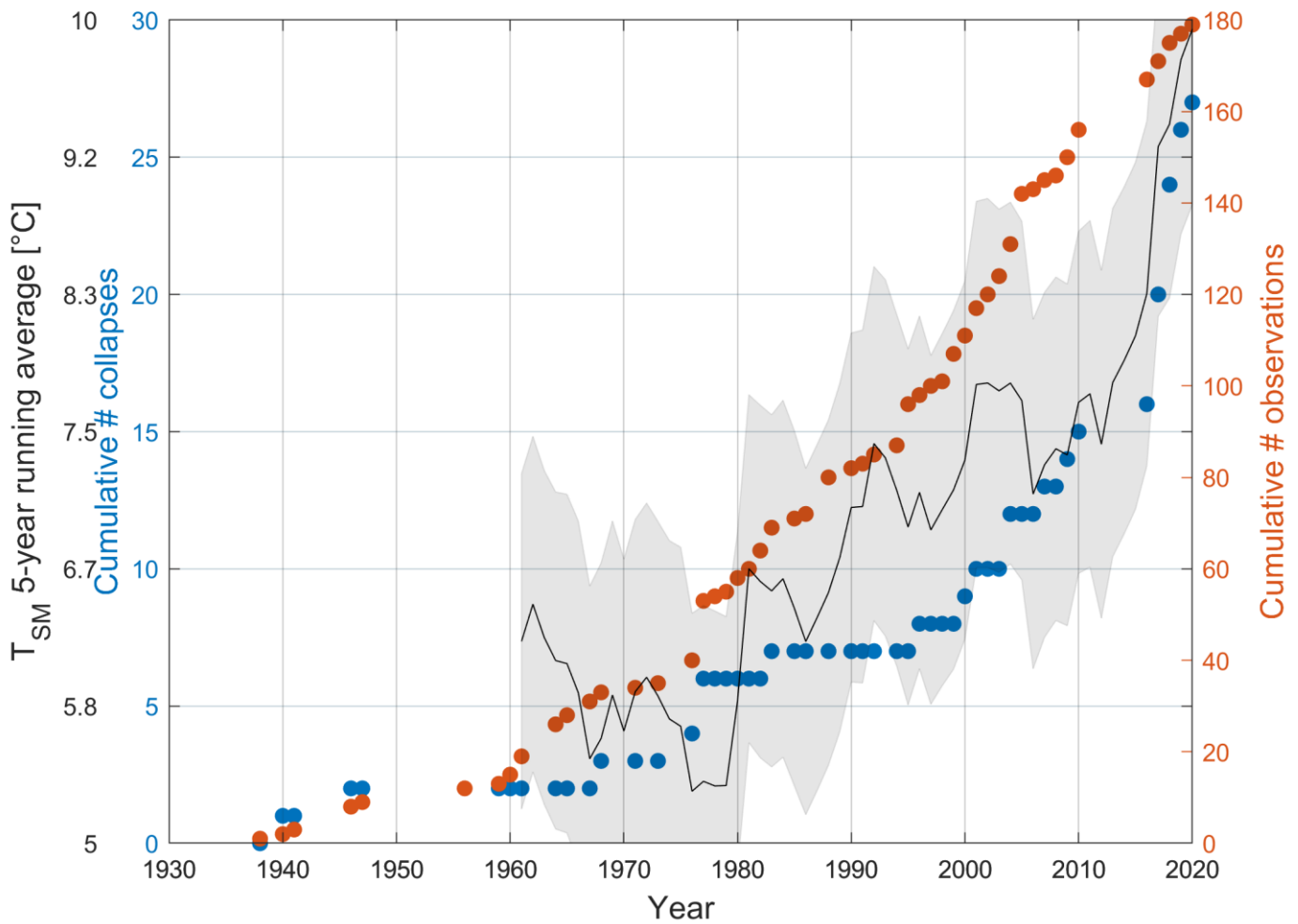


Figure 1: Composite image of aerial imagery of collapse features. (a) Glacier de Corbassière (2020, partly debris covered), (b) Glacier de Ferpècle (2016, partly debris covered), (c) Findelengletscher (2017, debris free), (d), Furgggletscher (2019, largely debris covered), (e) Gornergletscher (2006, partly debris covered), (f) Langgletscher (2017, largely debris covered), (g) Glacier de Moiry (2017, partly debris covered), (h) Oberaargletscher (2018, largely debris covered), (i) Glacier d’Otemma (2017, partly debris covered), (j) Turtmanngletscher (2017, debris free), (k) Unteraargletscher (2018, largely debris covered), (l) Glacier de Zinal (2016, largely debris covered)

265
266
267
268
269
270
271
272
273
274
275

276 Figure 2 shows the cumulative number of different collapse events observed on the
 277 aerial images, along with the cumulative number of observations, as a function of time
 278 from 1938 to present. The 5-year running average and standard deviation of the mean
 279 summer air temperature of all glaciers with collapse features are also displayed for
 280 comparison. We see that, as described previously, there is an increase in the frequency
 281 of observations starting in the early 1980s. Interestingly, however, the frequency of
 282 observed collapse events only starts to increase after the year 2000. Specifically, from
 283 the mid to late 1990s there is a substantial increase in the frequency of collapse events,
 284 and especially in the last 5 years, suggesting that as climate warming accelerates and
 285 as glacier retreat continues, so does the tendency for collapse features to form.
 286
 287



289 **Figure 2:** Cumulative number of collapse events (blue dots) and cumulative number
290 of observations (orange dots) since 1938 for all 22 glaciers considered in our study. 5-
291 year running average of the mean summer temperature (T_{SM} , black line) since 1961
292 over the 12 glaciers exhibiting one or several collapse events, along with the standard
293 deviation around the mean temperature (grey shaded area).

296 **3.2 Statistical analysis of collapse conditions**

297
298
299 Application of the Mann-Whitney U test with a 5% - 95% confidence interval to all 24
300 properties (Table S2) shows that the collapse and non-collapse groups of glaciers only
301 differ significantly with respect to five variables (Figure S2); (1) ice thickness near the
302 collapse area (Figure S2a); (2) estimated creep closure rate in the collapse area (Figure
303 S2b); (3) estimated ice flow velocity in the collapse area (Figure S2c); (4) the mean
304 surface slope within the collapse area (Figure S2d); and (5) the mean surface slope as
305 measured from the upstream edge to the downstream edge of the collapse area (Figure
306 S2e). These results suggest that relatively thin ice, a shallow surface slope and, a
307 function of these two parameters, low longitudinal flow velocity in the immediate vicinity
308 of a marginal subglacial channel are the conditions required for collapse. Ice having a
309 thickness of less than 50 m, for example, results in creep closure being small enough
310 that a subglacial channel with a diameter of 5 m does not close over winter (calculations
311 according to Supporting Information section 3.1; results for each glacier in Table S6).
312 Combined with a small surface slope (a median of 11.4° for glaciers with collapse
313 features; Table S6) and a small bed slope (a median of 14.3° for glaciers with collapse
314 features; Table S6) this shallow ice also results in very low estimated glacier-
315 longitudinal flux, further impeding channel closure. Retreat and ice thickness data are

316 displayed in Table S3 (further details are provided in Table S5), whereas the results of
317 the Mann-Whitney U test are displayed in Table S2.

320 **3.3 Relationship between summer air temperatures and retreat**

321
322 The mean annual retreat rate, the mean summer temperature in the snout zone in the
323 period during which each glacier was retreating, and the coefficient of variation of
324 retreat did not differ between glaciers exhibiting and not exhibiting collapse features.
325 However, glaciers with collapse features had systematically more negative correlations
326 between annual retreat and mean annual summer temperature ($p < 0.05$) and
327 significantly higher sensitivity of annual variations in glacier length to mean annual
328 summer temperature ($p < 0.05$) (Figure S11). For the glaciers with collapse features, 6
329 out of 12 had significant ($p < 0.05$) negative P_{RT} values compared with 2 out of 10 non-
330 collapse glaciers. Thus, a diagnostic feature of glaciers showing collapse features
331 appears to be a stronger sensitivity to mean summer temperature.

334 **3.4 Measurement of an active collapse at the Glacier d'Otemma**

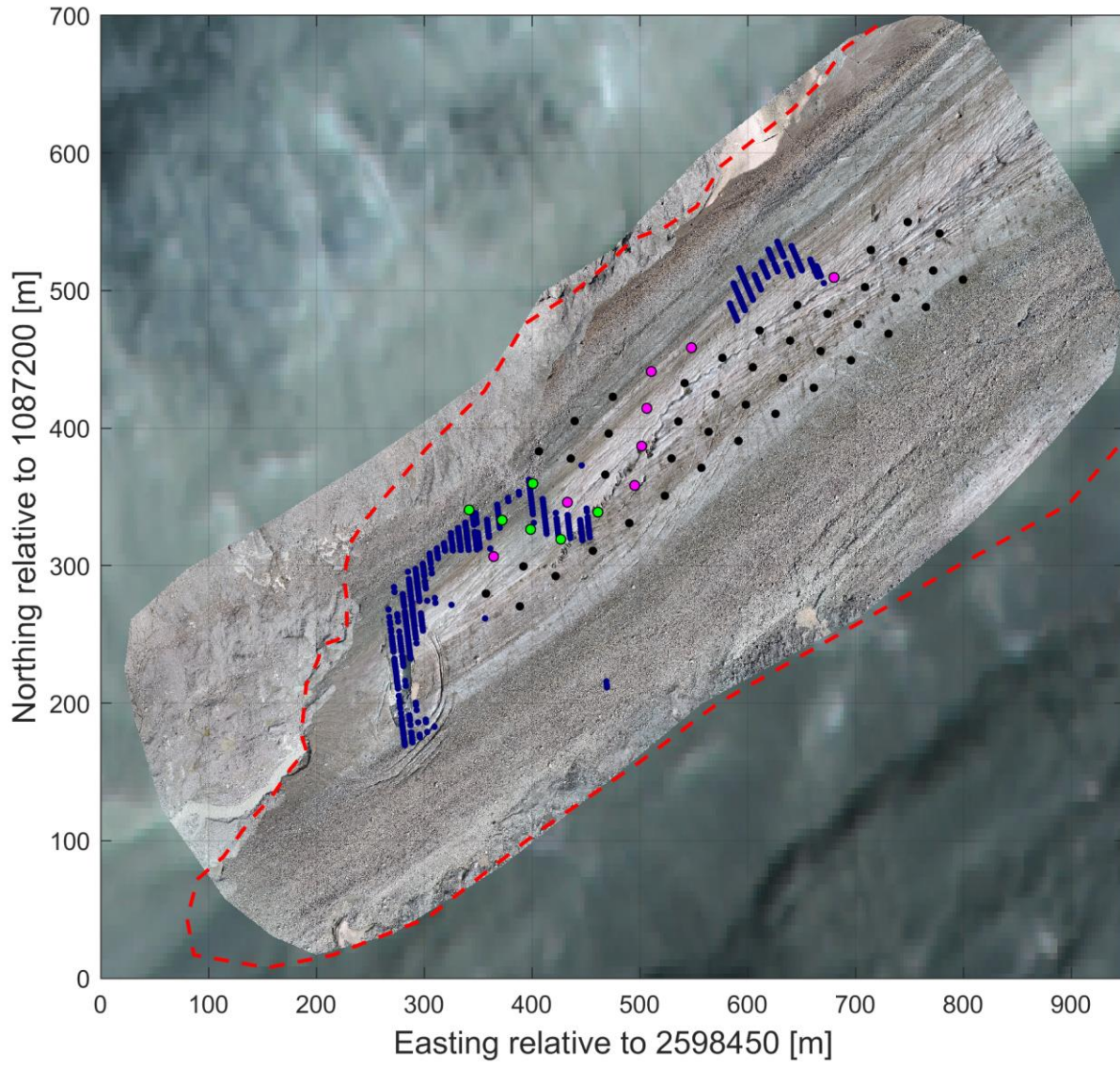
335
336 Figure 3a shows the UAV-based orthoimage of the Glacier d'Otemma that was taken on
337 August 7, 2018, upon which are superposed the positions of the ablation stakes and the
338 location of a 10-m-wide subglacial channel that was detected based on high-resolution
339 GPR data acquired a year earlier in August 2017 (Egli et al., 2021). The orthoimage
340 shows development of a collapse feature close to the snout of the glacier near the
341 downstream end of the identified channel.

342
343 Figure 3b shows the surface elevation changes that occurred between August 7 and 23,
344 2018. General surface height loss is observed all along the glacier tongue. This loss is
345 greatest (up to 1.2 m) in areas of bare ice and reduced where there is higher debris
346 cover (Figures 3a and 3b). Figure 3b also shows increased lowering of the surface above
347 the GPR-identified subglacial channel. Areas outside of the glacier outline show little

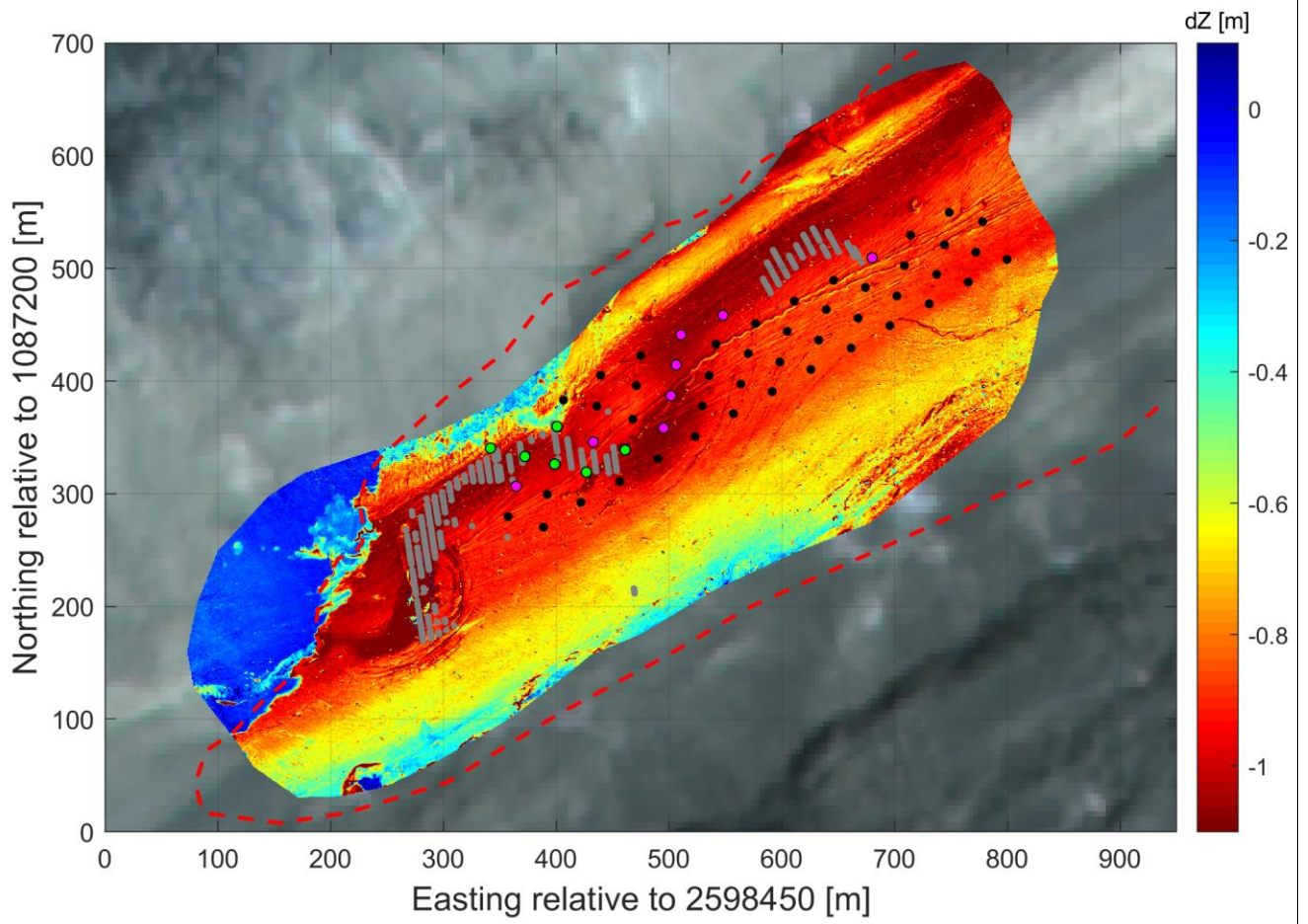
348 vertical change, with the exception for zones where 'dead ice' is melting under the debris
349 cover (e.g. at 200 m / 280 m relative Easting / Northing in Figure 3b). Figure 3c shows
350 the surface change after removal of the kriging-interpolated ablation stake
351 measurements. This results in some differences from the original DoD, but the pattern
352 of strong surface lowering in the vicinity of the subglacial channel persists. To rule out
353 factors other than the presence of a subglacial channel that may cause surface elevation
354 changes, we examined the correlations between surface change and the glacier surface
355 slope, reflectance, aspect and elevation for small patches (0.5 x 0.5 m) around each
356 ablation stake location. None of these four variables were correlated with elevation
357 change or ablation rate (Table S4, Figures S7 and S8). Thus, the surface change shown
358 in Figure 3c can be attributed to enhanced vertical deformation related to the presence
359 of a subglacial channel that must have been at atmospheric pressure; but where this
360 enhanced deformation was not sufficient for the channel to close and to become
361 pressurised.

362
363 Surface elevation changes and ablation measurements were compared for three
364 different categories defined according to position: locations known to be above the
365 identified subglacial channel (called on-channel), locations that are likely to be above
366 the channel (called likely on-channel), and locations that are off-channel (called off-
367 channel). A Mann-Whitney U test shows no significant difference ($p=0.05$) in ablation
368 between on-channel/likely-on and off-channel locations. With regard to surface
369 elevation changes, on the other hand, the Mann-Whitney U test shows that on-channel
370 values are significantly different from those at off channel stakes ($p<0.05$), whereas
371 likely on-channel values are not significantly different from off-channel values (Figure
372 S12, Table S5).

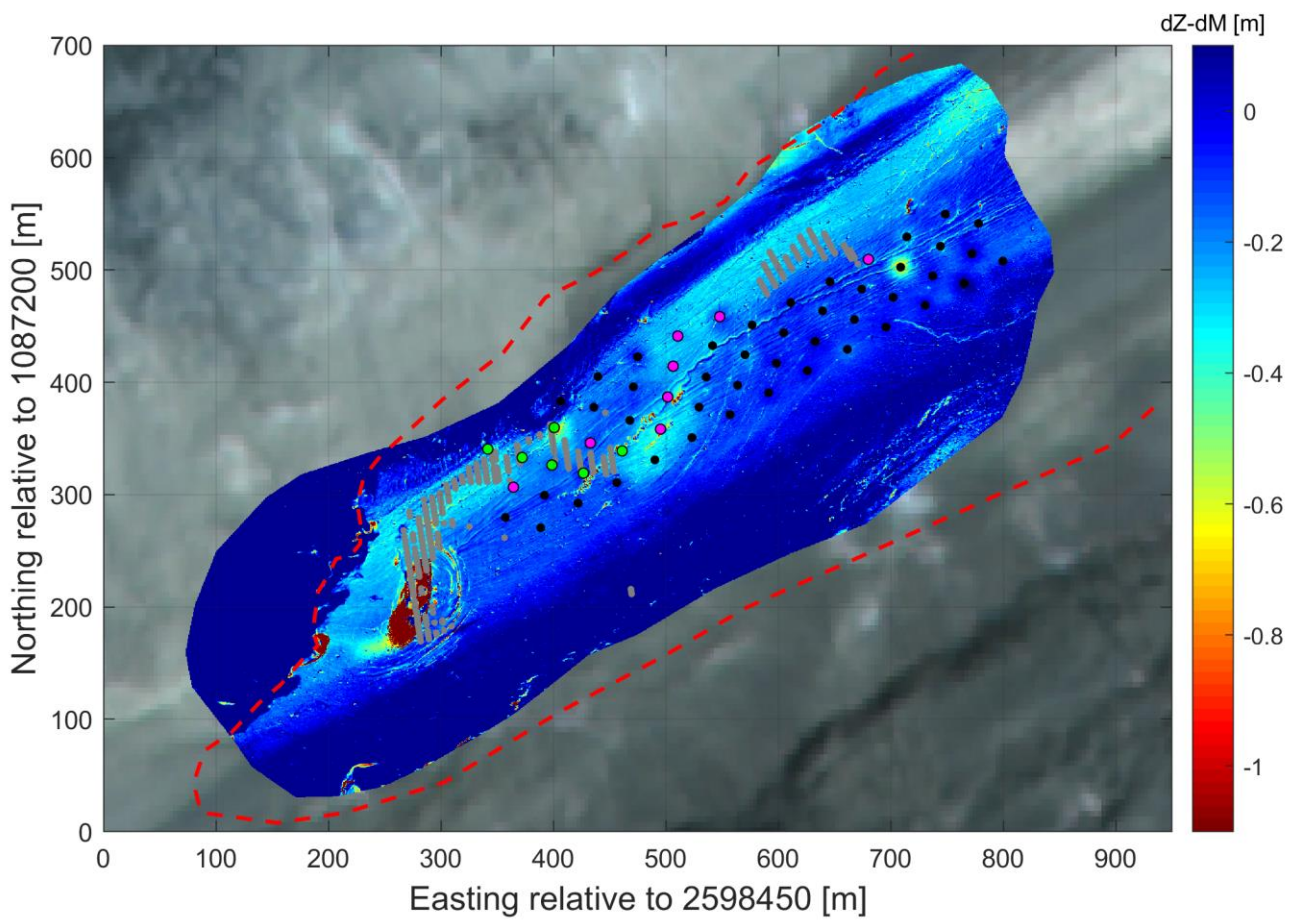




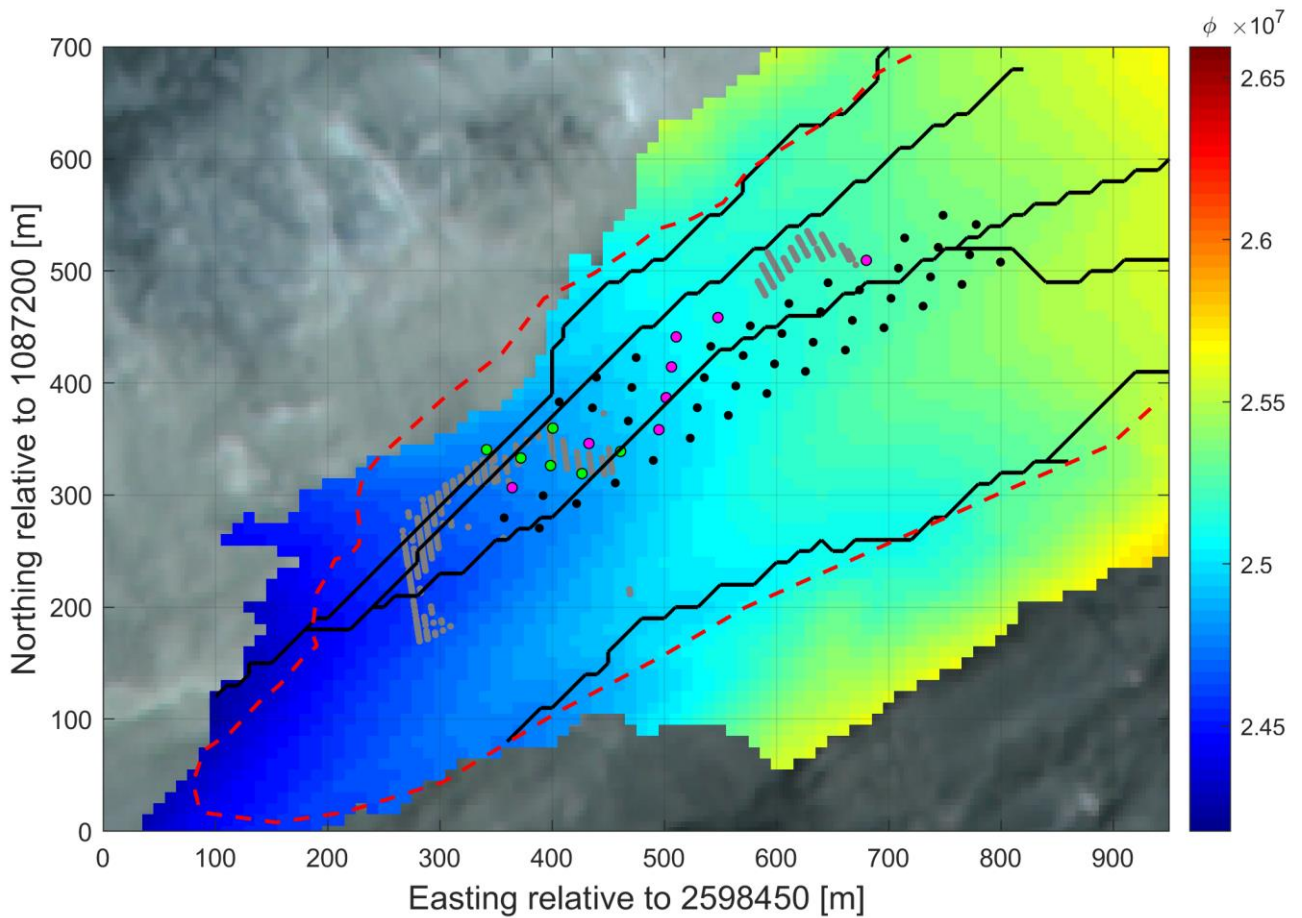
(a)



(b)



(c)



(d)

374

375

376

377

378

379

380

381

382

Figure 3: (a) Orthophoto with locations of ablation stakes (dots) and subglacial channel locations in blue stipples (b) Change in surface elevation (DoD) computed between August 7 and 23, 2018, overlain by subglacial channel positions (grey stipples) detected based on GPR data from August 2017 (Egli et al., 2021). The collapsed area is clearly visible at 280 m Easting / 200 m Northing. (c) Image in (b) after subtraction of ablation measurements. The ablation stakes are subdivided in

383 *different colors, where black is for stakes located off-channel, cyan is for stakes*
384 *located almost certainly on top of a subglacial channel (on-channel) and magenta is*
385 *for stakes likely to be located on-channel, according to a map of the Shreve potential*
386 *(Figure 6d) and to the proximity to the GPR-derived channels. Ablation was*
387 *interpolated using kriging in order to fit the grid cells of the DEMs. There are some*
388 *obvious local artifacts such as the point at 700 m Easting / 500 m Northing, but the*
389 *strong ablation pattern from the image in (b) is preserved.*

392 **4 Interpretation and discussion**

393
394 The analysis of historical imagery has revealed a systematic increase in the frequency
395 of surface collapse features due to 'subglacial stoping' or 'block caving' (Loewe, 1957;
396 Paige, 1956) in a set of Swiss glaciers since the mid to late 1990s (Figure 2) and about
397 5 to 10 years after the onset of rapid climate warming for this region (Costa et al.,
398 2018). Such a delay is not surprising as most Alpine glaciers show a lag in the onset of
399 retreat following a reduction in accumulation and an increase in ablation (Jouvet et al.,
400 2011). Although the examined glaciers differ significantly in properties such as size,
401 elevation range, and retreat rate, collapse features shown in Figure 1 were found
402 predominantly in those glaciers having margins comprised of thin ice (generally with a
403 thickness of less than 50 m; Table S3) and with shallow surface slopes and bed slopes
404 (both less than 23°; Table S6). Flow velocity calculations suggested that these were
405 zones of almost no longitudinal ice flux (Figure S2c, S2d) and reduced vertical channel
406 closure rates (Figure S2b).

407
408 Intensive investigation of one of the 12 glaciers with collapse features showed that the
409 collapse was centered directly over a subglacial channel. Remarkably, enhanced vertical
410 deformation was observed above this channel for at least 600 m up glacier (Figure 3b,
411 3c) Any void under a glacier should be subject to void-directed ice flow unless the water
412 pressure in the void equals the ice overburden pressure (Nye, 1953; Fountain and
413 Walder, 1998). The enhanced vertical deformation observed above the subglacial
414 channel at Otemma indicates that the latter was not the case for some way up-glacier.

415 Indeed, it is likely that this channel was at atmospheric pressure but that the vertical
416 deformation was not enough to close the void. Based on the analysis presented in Hooke
417 (1984, Figure 2) and with the thickness of ice at the snout of the glacier and a glacier
418 bed slope that is marginally greater than the glacier surface slope, the channel is likely
419 to be open. Our work importantly suggests that locally-increased vertical deformation
420 rates on Alpine glaciers may be used to map the position of such subglacial channels
421 flowing at atmospheric pressure.

422
423 The vertical deformation over the subglacial channel at the Glacier d'Otemma was
424 approximately 0.2 to 0.3 m over a 16 day period (Figure 3c). Theoretical calculations
425 using Hooke (1984) (Supplementary Information section 3.1) for the glacier suggested
426 a closure of 0.18 m per year if we assume a 5-m diameter semi-circular channel. One
427 explanation for a higher closure rate than predicted by the theory is that the channel is
428 wider and flatter than an assumed semi-circle, as has now been observed in boreholes
429 at the Glacier d'Otemma in summer 2021, and reported for Rhonegletscher (Church et
430 al., 2021). The analysis using the theory on shallow subglacial conduits by Hooke et al.
431 (1990) produces closure rate estimates over a 16-day period of ~ 0.03 to 0.13 m
432 (Supplementary Information section 3.5).

433
434 These theoretical estimates are much closer to, albeit still lower than, the measured
435 vertical deformation rate. The question then becomes why is it possible to maintain such
436 high vertical deformation rates without returning the subglacial channel to a pressurized
437 state? Field observations revealed large blocks of ice in the braid plain downstream from
438 the glacier during the collapse event. We propose that as the ice overlying the subglacial
439 channel close to the terminus is thin (~ 5 -7 m; Figure S13 in Supporting Information)
440 and as it creeps towards the channel, ice blocks may fall off the ceiling (block caving;
441 Paige, 1956). Thus, whilst there is an enhanced vertical deformation rate additional ice
442 is lost via subglacial caving rather than contributing to subglacial channel closure. These
443 findings are supported by the results of a study of more than 1400 Esker enlargements
444 assumed to indicate ice marginal subglacial channel collapse in the late stage of rapid
445 ice sheet retreat (Dewald et al., 2021).

447 There are two additional mechanisms that may play a role in the development of
448 collapse features and that merit further investigation. The first relates to the greater
449 sensitivity in the retreat of glaciers with collapse features to inter-annual summer
450 temperature variation (Figure S11b). This sensitivity could arise from reduced
451 longitudinal flux in the snout margin of such glaciers (Figure S2c), but it could also arise
452 because of enhanced subglacial exposure to warm air during summers. The measured
453 vertical deformation at the Glacier d'Otemma suggests a significant up-glacier extent of
454 water flow at atmospheric pressure (Figure 3b and 3c) and hence subglacial exposure
455 to the atmosphere and warm air incursion.

456
457 The second mechanism to note is suggested in Figure 3a, which shows that the
458 subglacial channel at the Glacier d'Otemma is meandering and that the collapse feature
459 forms at a bend in the channel.

460
461 The time-series images of collapse at the Otemma glacier shows that the collapse
462 morphology has meander-parallel crevasses (Figure S15). The possibility that subglacial
463 channels are sinuous has been recognized, notably in studies of dye breakout curves
464 (Kohler, 1995) suggesting the presence of open-channel flow with walls comprised of
465 ice and/or till that can be mechanically eroded. It is well-established that straight rivers
466 that are able to erode their beds and/or banks tend to initiate meandering as a result
467 of the inherent instability related to the effects of turbulent anisotropy on secondary
468 circulation and which tends to grow as a function of time across a wide range of river
469 scales (Dey and Ali, 2017). In theory, deviation from a glacier-longitudinal orientation
470 exposes the channel to greater longitudinal fluxes and hence greater closure so meaning
471 that subglacial channels can't meander unless they can erode into bedrock. The margins
472 of temperate Alpine glaciers are commonly zones of ice compression (Hart, 1995) as a
473 zone of colder surface ice in the ablation zone connects with the bed at the snout margin
474 (Moore et al., 2009). This would also aid closure of non-longitudinally-oriented channels.
475 At the Otemma glacier with the estimated longitudinal velocities (1.29 m per year, Table
476 S4) the 10-m-wide subglacial channel would only close by around 10 to 15% per year.
477 This would allow maintenance of channels that meander. Thus, as glaciers thin and their
478 longitudinal velocities fall, not only do subglacial channels close less readily, they may

479 be increasingly able to maintain a meandering form. As technologies for mapping
480 subglacial channels improve, it should become possible to test the hypothesis that the
481 formation of meandering open channel flow under glacier snout margins with low
482 longitudinal ice flux is a contributory mechanism to the onset of collapse.

483
484 Our wider statistical analysis suggests that glaciers with collapse features tend to have
485 lower rates of longitudinal flux and so reduced compression and longitudinal closure
486 (Figure S2f). Low longitudinal flux is a consequence of short-term increases in ablation
487 and glacier thinning and long-term reduction of flux of accumulated ice into the ablation
488 zone, both a consequence of climate warming. This explains the increased frequency of
489 glacier collapse events (Figure 1) and that such events are likely to be a more frequent
490 occurrence at Alpine glacier margins as climate warming continues.

493 **Acknowledgments, Samples, and Data**

- 494 • This project was funded by the Canton de Vaud. We thank the authorities of the
495 Commune de Bagnes for granting access to the field site. We acknowledge Dr.
496 Andreas Bauder, Dr. Mauro Werder, and Dr. Daniel Farinotti from VAW at ETH
497 Zurich for providing us with the most recent Swiss ice thickness and bed
498 topography datasets.
- 499 • No real or perceived financial conflicts of interest are present for this article.
- 500 • None of the authors has an affiliation that may present a conflict of interest for
501 this article.
- 502 • The data supporting the conclusions meets FAIR principles and is supplied with
503 this paper for the purposes of review under the following link:
504 [https://datadryad.org/stash/share/Ig5BhqwviMUgdDaLt-](https://datadryad.org/stash/share/Ig5BhqwviMUgdDaLt-kP3FB_giWPZRBqMC0cvfNzKA4)
505 [kP3FB_giWPZRBqMC0cvfNzKA4](https://datadryad.org/stash/share/Ig5BhqwviMUgdDaLt-kP3FB_giWPZRBqMC0cvfNzKA4) .

508 **References**

509
510 Bartholomaeus, T. C., Anderson, R. S., & Anderson, S. P. (2011). Growth and collapse
511 of the distributed subglacial hydrologic system of Kennicott Glacier, Alaska, USA, and
512 its effects on basal motion. *Journal of Glaciology*, 57, 985-1002.

513

514 Church, G., Bauder, A., Grab, M., & Maurer, H. (2021). Ground-penetrating radar
515 imaging reveals glacier's drainage network in 3D. *The Cryosphere*, 15, 3975–3988,
516 <https://doi.org/10.5194/tc-15-3975-2021>

517

518 Costa, A., Molnar, P., Stutenbecker, L., Bakker, M., Silva, T. A., Schlunegger, F., ... &
519 Girardclos, S. (2018). Temperature signal in suspended sediment export from an
520 Alpine catchment. *Hydrology and earth system sciences*, 22, 509-528.

521

522 Cuffey, K. M., & Paterson, W. S. B. (2010). *The physics of glaciers*. Academic Press.

523

524 Cutler, P. M. (1998). Modelling the evolution of subglacial tunnels due to varying
525 water input. *Journal of Glaciology*, 44, 485-497.

526

527 Dewald, N., Lewington, E. L. M., Livingstone, S. J., Clark, Ch. D. & Storrar, R. D.
528 (2021). Distribution, Characteristics and Formation of Esker Enlargements.
529 *Geomorphology*, <https://doi.org/10.1016/j.geomorph.2021.107919>.

530

531 Dey, S., & Ali, S. Z. (2017). Origin of the onset of meandering of a straight river.
532 *Proceedings of the Royal Society A: Mathematical, Physical and Engineering Sciences*,
533 473, Article number 20170376.

534

535 Egli, P., Irving, J., & Lane, S. (2021). Characterization of subglacial marginal channels
536 using 3-D analysis of high-density ground-penetrating radar data. *Journal of*
537 *Glaciology*, 67, 759-72

538

539 Fountain, A. G., & Walder, J. S. (1998). Water flow through temperate glaciers.
540 *Reviews of Geophysics*, 36, 299-328.

541

542 Gantayat, P., Kulkarni, A. V., & Srinivasan, J. (2014). Estimation of ice thickness using
543 surface velocities and slope: case study at Gangotri Glacier, India. *Journal of*
544 *Glaciology*, 60, 277-282.

545

546 Gindraux, S., Boesch, R., & Farinotti, D. (2017). Accuracy assessment of digital
547 surface models from unmanned aerial vehicles' imagery on glaciers. *Remote Sensing*,
548 9, Article number 186.

549

550 GLAMOS (1881-2019), The Swiss Glaciers 1880-2016/17, Glaciological Reports No 1-
551 138, Yearbooks of the Cryospheric Commission of the Swiss Academy of Sciences
552 (SCNAT), published since 1964 by VAW / ETH Zurich, doi:10.18752/glrep_series.

553

554 Glen, J. W. (1958). The flow law of ice: A discussion of the assumptions made in
555 glacier theory, their experimental foundations and consequences. *IASH Publ*, 47,
556 e183.

557

558 Grab, M., Mattea, E., Bauder, A., Huss, M., Rabenstein, L., Hodel, E., ... & Maurer, H.
559 (2021). Ice thickness distribution of all Swiss glaciers based on extended ground-

- 560 penetrating radar data and glaciological modeling. *Journal of Glaciology*, First View: 1-
561 19.
- 562
- 563 Hooke, R. L. (1984). On the role of mechanical energy in maintaining subglacial water
564 conduits at atmospheric pressure. *Journal of Glaciology*, 30, 180-187.
- 565
- 566 Haeberli, W., & Hölzle, M. (1995). Application of inventory data for estimating
567 characteristics of and regional climate-change effects on mountain glaciers: a pilot
568 study with the European Alps. *Annals of Glaciology*, 21, 206-212.
- 569
- 570 Hart, J. K. (1995). An investigation of the deforming layer/debris-rich basal-ice
571 continuum, illustrated from three Alaskan glaciers. *Journal of Glaciology*, 41(139),
572 619-633.
- 573
- Huss, M., Jouvett, G., Farinotti, D., & Bauder, A. (2010). Future high-mountain
hydrology: a new parameterization of glacier retreat. *Hydrology and Earth System
Sciences*, 14, 815-829.
- 574 Hooke, R. L. (1984). On the role of mechanical energy in maintaining subglacial water
575 conduits at atmospheric pressure. *Journal of Glaciology*, 30, 180-187.
- 576
- 577 Hooke, R. L., Laumann, T., & Kohler, J. (1990). Subglacial water pressures and the
578 shape of subglacial conduits. *Journal of Glaciology*, 36, 67-71.
- James, M. R., Antoniazza, G., Robson, S., & Lane, S. N. (2020). Mitigating systematic
error in topographic models for geomorphic change detection: accuracy, precision and
considerations beyond off-nadir imagery. *Earth Surface Processes and Landforms*, 45,
2251-2271.
- James, M. R., Chandler, J. H., Eltner, A., Fraser, C., Miller, P. E., Mills, J. P., ... &
Lane, S. N. (2019). Guidelines on the use of structure-from-motion photogrammetry in
geomorphic research. *Earth Surface Processes and Landforms*, 44, 2081-2084.
- James, M. R., Robson, S., & Smith, M. W. (2017). 3-D uncertainty-based topographic
change detection with structure-from-motion photogrammetry: precision maps for
ground control and directly georeferenced surveys. *Earth Surface Processes and
Landforms*, 42, 1769-1788.
- 579 Jarque, C.M. and Bera, A.K., 1980. Efficient tests for normality, homoscedasticity and
580 serial independence of regression residuals. *Economics Letters*, 6, 255-259
- 581
- 582 Jouvett, G., Huss, M., Funk, M., & Blatter, H. (2011). Modelling the retreat of Grosser
583 Aletschgletscher, Switzerland, in a changing climate. *Journal of Glaciology*, 57, 1033-
584 1045.
- Kellerer-Pirklbauer, A., and Kulmer, B. (2019) The evolution of brittle and ductile
structures at the surface of a partly debris-covered, rapidly thinning and slowly moving

glacier in 1998–2012 (Pasterze Glacier, Austria), *Earth Surf. Process. Landforms*, 44, 1034– 1049.

Kohler, J. (1995). Determining the extent of pressurized flow beneath Storglaciären, Sweden, using results of tracer experiments and measurements of input and output discharge. *Journal of Glaciology*, 41, 217-231.

585

586 Konrad, S. K. (1998). Possible outburst floods from debris-covered glaciers in the
587 Sierra Nevada, California. *Geografiska Annaler: Series A, Physical Geography*, 80,
588 183-192.

589

590 Lindström, E (1993) Esker enlargements in Northern Sweden, *Geografiska Annaler:*
591 *Series A, Physical Geography*, 75, 95-110

592

593 Loewe, F. (1957). Subglacial stoping or block caving. *Journal of Glaciology*, 3, 152-
594 152.

595

596 Mann, H.B., Whitney, D.R., 1947. On a test of whether one of two Random variables is
597 stochastically larger than the other. *Annals of Mathematical Statistics*, 18, 50–60.

598

599 Moore, P. L., Iverson, N. R., & Cohen, D. (2009). Ice flow across a warm-based/cold-
600 based transition at a glacier margin. *Annals of Glaciology*, 50, 1-8.

601

602 Nienow, P., Sharp, M., & Willis, I. (1998). Seasonal changes in the morphology of the
603 subglacial drainage system, Haut Glacier d'Arolla, Switzerland. *Earth Surface*
604 *Processes and Landforms*, 23, 825-843.

605

606 Nye, J. F. (1953). The flow law of ice from measurements in glacier tunnels,
607 laboratory experiments and the Jungfraufirn borehole experiment. *Proceedings of the*
608 *Royal Society of London. Series A. Mathematical and Physical Sciences*, 219, 477-489.

609

Paul, F., Azzoni, R.S., Fugazza, D., Le Bris, R., Nemec, J., Paul, F., Rabatel, A.,
Ramusovic, M., Rastner, Ph., Schaub, Y., Schwaizer (née Bippus), G. (2019) *GLIMS*
Glacier Database. Boulder, CO. National Snow and Ice Data Center.
<http://dx.doi.org/10.7265/N5V98602>

Paul, F., & Haeberli, W. (2008). Spatial variability of glacier elevation changes in the
Swiss Alps obtained from two digital elevation models. *Geophysical Research Letters*,
35, L21502

610

611 Paige, R. (1956). Subglacial stoping or block caving: a type of glacier ablation. *Journal*
612 *of Glaciology*, 2, 727-729.

613

614 Rippin, D. M., Pomfret, A., & King, N. (2015). High resolution mapping of supra-glacial
615 drainage pathways reveals link between micro-channel drainage density, surface
616 roughness and surface reflectance. *Earth Surface Processes and Landforms*, 40, 1279-
617 1290.

618

619 Rossini, M., Di Mauro, B., Garzonio, R., Baccolo, G., Cavallini, G., Mattavelli, M.,...,
620 Colombo, R. (2018). Rapid melting dynamics of an alpine glacier with repeated uav
621 photogrammetry. *Geomorphology*, 304, 159-172.

622
623 Salzmann, N., Machguth, H., & Linsbauer, A. (2012). The Swiss Alpine glaciers'
624 response to the global '2° C air temperature target'. *Environmental Research Letters*,
625 7, 044001.

626
627 Shreve, R. L. (1972). Movement of water in glaciers. *Journal of Glaciology*, 11, 205-
628 214.

629
630 Stocker-Waldhuber, M., Fischer, A., Keller, L., Morche, D., & Kuhn, M. (2017). Funnel-
631 shaped surface depressions—indicator or accelerant of rapid glacier disintegration? A
632 case study in the Tyrolean Alps. *Geomorphology*, 287, 58-72.

633
634 SwissTopo (2021), <https://map.geo.admin.ch>

635
636 Westoby, M. J., Brasington, J., Glasser, N. F., Hambrey, M. J., & Reynolds, J. M.
637 (2012). 'structure-from-motion' photogrammetry: A low-cost, effective tool for
638 geoscience applications. *Geomorphology*, 179, 300-314.

639
640 Zekollari, H., Huss, M., & Farinotti, D. (2019). Modelling the future evolution of
641 glaciers in the European Alps under the EURO-CORDEX RCM ensemble. *The*
642 *Cryosphere*, 13, 1125-1146.

643